Front. Struct. Civ. Eng. 2022, 16(11): 1436–1452
https://doi.org/10.1007/s11709-022-0889-y

RESEARCH ARTICLE

Assessment and prediction of the mechanical properties of ternary geopolymer concrete

Jinliang LIU*, Wei ZHAO, Xincheng SU, Xuefeng XIE

School of Civil Engineering, Northeast Forestry University, Harbin 150040, China
**Corresponding author. E-mails: jinliangliu@nefu.edu.cn; jinliangliu_2015@126.com*

ABSTRACT This paper utilized granulated blast furnace slag (GBFS), fly ash (FA), and zeolite powder (ZP) as the binders of ternary geopolymer concrete (TGC) activated with sodium silicate solution. The effects of alkali content (AC) and alkaline activator modulus (AAM) on the compressive strength, flexural tensile strength and elastic modulus of TGC were tested and the SEM micrographs were investigated. The experimental results were then compared with the predictions based on models of mechanical properties, and the amended models of TGC were proposed taking account of the effects of AC and AAM. The results indicated that increasing AC and reducing AAM which were in the specific ranges (5% to 7% and 1.1 to 1.5, respectively) had positive effects on the mechanical properties of TGC. In addition, the flexural tensile strength of TGC was 27.7% higher than that of OPC at the same compressive strength, while the elastic modulus of TGC was 25.8% lower than that of OPC. Appropriate prediction models with the R^2 of 0.945 and 0.987 for predicting flexural tensile strength and elastic modulus using compressive strength, respectively, were proposed. Fitting models, considering the effects of AC and AAM, were also proposed to predict the mechanical properties of TGC.

KEYWORDS Ternary Geopolymer Concrete (TGC), alkaline activator modulus, alkali content, mechanical properties, assessment

1 Introduction

The process of manufacturing cement causes serious issues such as environmental pollution and huge consumption of energy [1,2]. In general, producing 1 tonne Ordinary Portland cement (OPC) releases many pollutants such as particles, nitrogen oxides and carbon dioxide [3]. Therefore, it is inevitable to explore a sustainable alternative to OPC to ease the burden on the environment. Geopolymer is an environment-friendly cementitious material utilized in the civil engineering industry to prepare high-performance concrete, and the industry aims at replacing OPC with geopolymer [4]. Geopolymer is a semi-crystalline inorganic cementitious material formed in a geopolymerization reaction with incorporation of alkaline activator and aluminosilicate precursor. The material offers a lot of advantages, such as better mechanical properties, stronger durability characteristics, lower shrinkage and lower density-to-strength ratio compared with OPC [5–11]. Various industrial products (metakaolin, zeolite and so on) and by-products (slag, fly ash, and so on) utilized as precursors have potential to provide raw material for synthesis of geopolymer [12–16]. Geopolymer has attracted particular worldwide attention in recent years due to its ability of making industrial waste profitable.

Due to the excellent pozzolanic activities, granulated blast furnace slag (GBFS) and fly ash (FA) are the most common industrial by-products used in producing geopolymer. GBFS is an industrial by-product from blast furnace iron-making process [17]. FA is a kind of small particle from the burning of fuels (mostly coal); it can, for instance, be collected from flue gas of coal power plants [18]. Producing 1 tonne big iron will generate 30% GBFS and consuming 1 tonne coal will produce 50% FA. As industrial residues, GBFS and FA with such large outputs can be hazardous to human health and atmosphere if they are released into the environment, hence the necessity of disposing of these wastes [19]. GBFS plays the role in enhancing the early strength of concrete thanks to its high

Article history: Received May 2, 2022; Accepted Jul 14, 2022

pozzolanic activity, large reactant surface area and high calcium content. All these factors contribute to high early strength due to the generation of hydration product C-(A)-S-H [20]. FA makes concrete easy to set and cast because of its eminent workability [21].

Zeolite power (ZP) is an environmentally friendly material and it is abundantly available due to its considerable yield worldwide and lower cost than other building materials [22,23]. ZP, with chief compositions of SiO_2 and Al_2O_3, is ground from natural zeolite; it is not industrial residue and it was first used in 1756 [24]. It has been confirmed that ZP contains silica with higher activity than FA [25–27]. ZP has a structure with rough surface and many internal pores [27]. It plays two primary roles in the concrete system: the first is as a "micro-pump"; ZP can store superfluous water in the early stage and discharge the internal water during the hardening process of concrete to further promote the hydration reaction, so as to enhance the later strength. The second is to provide more hydration space. There are many voids and pores in ZP, which can be considered as containers to provide space for the hydration reaction; meanwhile the hydration reaction products can fill the voids and pores, thus making the structure more stable and denser. Its corrosion resistance of the concrete is also improved [22]. Therefore, ZP has potential to increase strength of GBFS-FA geopolymer concrete as an enhancer.

As factors in the preparation of geopolymer, the selection and utilization of activators affect various properties of geopolymer such as mechanical property and durability [6,7]. The types of activators can be divided into acidic activator, saline activator and alkaline activator [28–32], among which the most widely used is alkaline activator. Alkaline activators can be further classified into two categories (potassium activator and sodium activator) according to different types of metallic cation, of which the most common is sodium activator [33]. The sodium-based activator can be made of sodium hydroxide, sodium silicate and a mixture of these [34–36]. The mechanical properties of geopolymer prepared with mixture of sodium hydroxide and sodium silicate are excellent [37]. Cho et al. [38] found that when AC in the activator ranged from 4% to 10%, and with a constant AAM of 1.4, the strength of FA based geopolymer increased with the increase of AC in the activator. The strength at the age of 28 days increased to 348% when AC increased from 4% to 6%. Fernández-Jiménez and Palomo [39] found that when AAM was selected at 1.23 and AC was 7.74%, the compressive strength of FA based geopolymer mortar at the age of 28 d can reach to a high level of 82.36 MPa. Criado et al. [40] reported that the activation effect on the synthesis of geopolymer is satisfactory; in the case of AAM it is between 1.0–1.5, in general.

Most previous investigations have been conducted with respect to mechanical properties of alkali-activated geopolymer concrete produced with various parameters of alkaline activator solution such as concentration of sodium hydroxide, amount of alkaline liquid and ratio of sodium silicate to sodium hydroxide [41–43]. However, there is scanty study on the variation of mechanical properties of GBFS-FA-ZP blended ternary geopolymer concrete (TGC) activated with different AAM and AC curing at room temperature. Therefore, in this study, two parameters of alkaline activator solution (AAM and AC) and constant proportions of GBFS, FA and ZP were chosen to investigate mechanical properties of TGC. SEM was conducted to observe the microstructure of TGC. Finally, the prediction models were proposed to assess and predict the mechanical properties of TGC. The study on TGC has promise to provide the theoretical basis for reusing hazardous industrial by-products and so to lighten the burden on the environment. In addition, promoting the application of this eco-friendly concrete could reduce cement production which has the potential to reduce the emission of carbon dioxide.

2 Materials and methods

2.1 Materials

2.1.1 Granulated blast furnace slag, fly ash and zeolite power

This paper utilized GBFS, FA, and ZP (Fig. 1) as aluminosilicate materials and the compositions of these materials are summarized in Table 1. GBFS deriving from Shijiazhuang, Hebei was S95 grade with higher content of CaO. FA stemming from Zhengzhou, Henan was secondary grade composed of the minerals crystalline quartz and mullite. ZP purchased from Shijiazhuang, Hebei was made by grinding natural zeolites with high content of SiO_2. XRD (X-ray Diffraction) test were conducted on each of these three materials after preparation as follows. First, the raw material powder was added into the middle of the groove of the sample rack to make the loose sample powder moderately higher than the plane of the sample rack. Then, the sample surface was gently pressed by using the slide, so that the powder sample surface was leveled and consistent with the frame plane, and the excess powder that was not in the groove was scraped off. Eventually, the sample was put into X-ray diffractometer for analysis. The XRD spectra of GBFS, FA, and ZP are shown in Fig. 2. A detectable peak in Fig. 2 indicated that the GBFS was composed of amorphous phases containing calcite. It can be observed in Fig. 2, that the FA consisted primarily of amorphous phases with some crystalline

phases (quartz and mullite). ZP was mainly composed of clinoptilolite crystalline phases. In addition, calcite ($CaCO_3$) could be detected despite low-intensity peaks, as presented in Fig. 2(c). In order to investigate microstructures of these aluminosilicate materials, a scanning electron microscope (SEM) was employed. SEM micrographs of GBFS, FA, and ZP are shown in Fig. 3, which shows that the particles of GBFS were irregular and had lots of edges and corners. The particles of FA with different sizes were all spherical, and their surfaces were smooth. The particles of ZP were very rough and more irregular than the GBFS particles. The particle size distribution curves of GBFS, FA, and ZP are shown in Fig. 4.

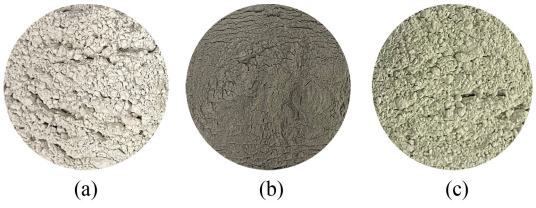

Fig. 1 Aluminosilicate materials: (a) GBFS, (b) FA, and (c) ZP.

Table 1 Chemical compositions of GBFS, FA, and ZP

material	SiO_2	CaO	Al_2O_3	Fe_2O_3	MgO	TiO_2	K_2O	Na_2O
GBFS (%)	42.12	40.20	16.04	0	0	0	0	0
FA (%)	56.96	1.50	23.67	4.63	1.50	0	0	0
ZP (%)	64.39	4.17	12.82	1.58	0.98	0.18	1.68	1.14

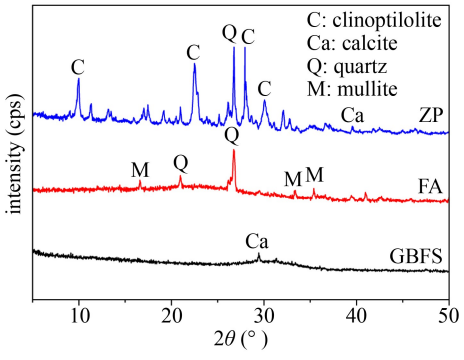

Fig. 2 XRD diffractograms of GBFS, FA, and ZP.

2.1.2 Activator

In order to activate the above aluminosilicate materials, this study selected industrial sodium silicate (water glass) solution (Fig. 5) with a SiO_2/Na_2O ratio of 3.47 (SiO_2 = 24.71%, Na_2O = 7.29%, H_2O = 68%) as alkaline activator. The 98% purity sodium hydroxide flakes (Fig. 5) were mixed with initial sodium silicate solution to reduce the ratio of SiO_2/Na_2O. The chemical reaction process is shown in Eq. (1):

$$2NaOH = Na_2O + H_2O. \quad (1)$$

The content of Na_2O in sodium silicate solution can be augmented by the above chemical reaction process, thereby reducing the ratio of SiO_2/Na_2O. The detailed preparation processes are as follows. Sodium hydroxide flakes are dissolved in water firstly. Then the sodium silicate solution is mixed with sodium hydroxide solution. Eventually, the mixed alkaline activator solution is left to stand for 24 h in order to dissipate the excessive heat [44]. The flow chart for preparing target water glass solution is presented in Fig. 6. In this paper, target moduli were 0.9, 1.0, 1.1, 1.2, 1.3, 1.4, and 1.5.

2.1.3 Aggregate

The fineness of river sand as the fine aggregate was 2.2. The size distributions of coarse aggregate were in two ranges: a) from 5 to 10 mm and b) 10 to 20 mm with a ratio of a:b of 0.67. Aggregates were used with a fine to coarse aggregate ratio of 0.4. The particle size distribution curves of fine aggregate and coarse aggregate are plotted in Fig. 7.

2.2 Methods

2.2.1 Mix proportioning design

This paper selected 65%GBFS, 25%FA, and 10%ZP [24,45–49] as aluminosilicate materials, and the liquid to solid ratio was 0.4. The AAM and AC of alkaline activator were used as variables. The mix proportioning of TGC was designed by controlling one variable

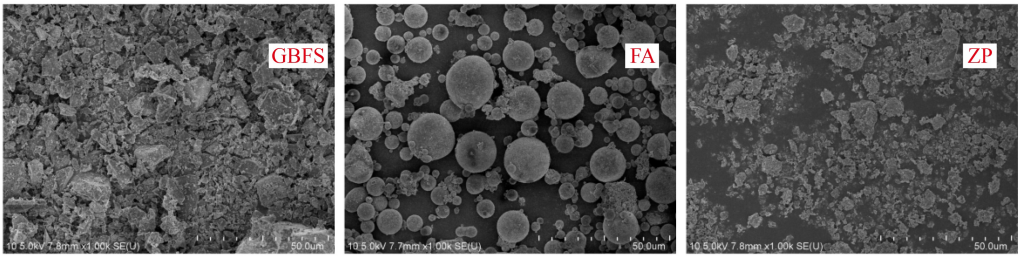

Fig. 3 SEM micrographs of GBFS, FA, and ZP.

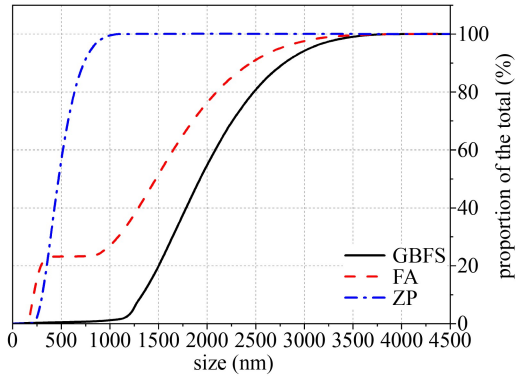

Fig. 4 Particle size distribution curves of GBFS, FA, and ZP.

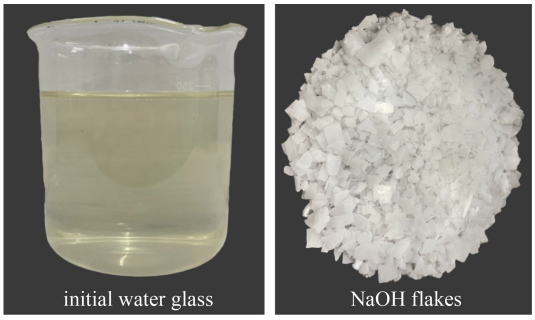

Fig. 5 (a) Initial water glass and (b) sodium hydroxide flakes.

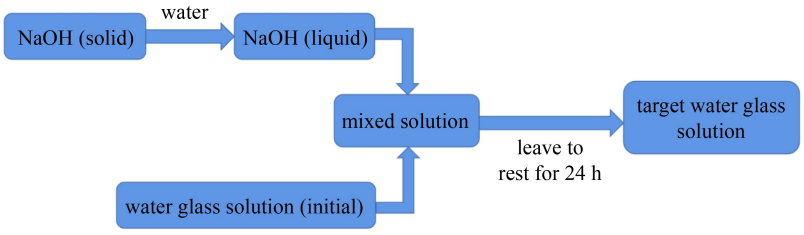

Fig. 6 The preparation flow chart of target water glass solution.

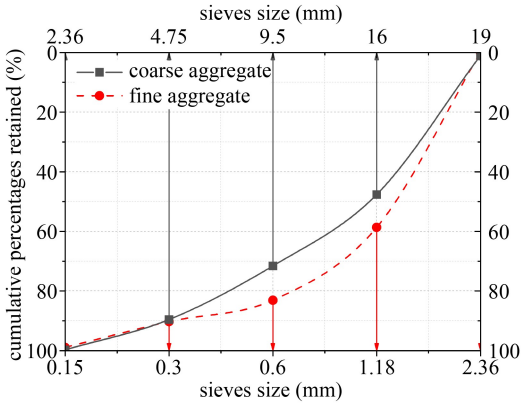

Fig. 7 The particle size distribution curves of fine aggregate and coarse aggregate.

unchanged and changing the other variable. When AAM was fixed at 1.4, the proportions of AC of alkaline activator were 5%, 5.5%, 6%, 6.5%, 7%, 8%, and 9% [38,39]. When AC was fixed at 8 %, AAM values were 0.9, 1.0, 1.1, 1.2, 1.3, 1.4, and 1.5 [40]. The details of mix proportions are shown in Table 2.

Table 2 Details of mix proportions

mix	total binders (kg/m^3)	AAM	AC (%)	fine aggregate (kg/m^3)	coarse aggregate (kg/m^3)
T1	380	1.4	5	720	1080
T2			5.5		
T3			6		
T4			6.5		
T5			7		
T6			8		
T7			9		
T8		0.9	8		
T9		1.0			
T10		1.1			
T11		1.2			
T12		1.3			
T13		1.5			

2.2.2 Preparation process for ternary geopolymer concrete

In order to prepare TGC specimens, according to GBT 50081-2019 [50], the aggregate, geopolymer precursors and alkaline activator solution were added into concrete mixer successively for stirring. After adequate mixing, the molds filled with TGC were put on a vibrating table to compact the concrete. After vibration, the molds were placed on a horizontal table for curing at ambient conditions with a temperature of (20 ± 5) °C and a relative humidity greater than 50%. After curing for 24 h, the samples were de-molded and put into the concrete standard curing room with a temperature of (20 ± 2) °C and a relative humidity greater than 95% to cure for 28 d.

2.2.3 Arrangement for test

Compression tests were conducted on thirty-nine

100 mm × 100 mm × 100 mm concrete cubes with a loading rate of 0.6 MPa·s^{-1}. Flexural tensile tests were conducted on thirty-nine 100 mm × 100 mm × 400 mm concrete prisms with a loading rate of 0.06 MPa·s^{-1}. Elastic modulus tests were conducted on seventy-eight 100 mm × 100 mm × 300 mm concrete prisms with a loading rate of 0.6 MPa·s^{-1}. All these tests were conducted in accordance with GBT 50081-2019 [50]. The diagrammatic sketches of compression test, flexural tensile test and elastic modulus test were plotted in Fig. 8.

The above mechanical property tests were carried out on a universal testing machine. The surface moisture of cured concrete samples was wiped dry before the test, and the tests were carried out immediately. The testing arrangement and failure pattern of TGC specimen under compression test and flexural tensile test are presented in Figs. 9, and 10, respectively.

3 Experimental results

3.1 Compressive strength and flexural tensile strength

Figure 11 shows the 28 d compressive strengths and flexural tensile strengths of TGC prepared under the condition of constant AAM with variable AC. According to the data showed in Fig. 11, it is apparent that the compressive strength and flexural tensile strength of mix T1 were both the lowest compared to those of other specimens. The specimen of T1 had the minimum compressive strength and flexural tensile strength of 56.9 and 5.6 MPa, respectively. When the AC proportion reached 7%, the compressive strength and flexural tensile strength of TGC specimen were both the highest compared to those of other specimens. The specimen of T5 obtained the maximum compressive strength and flexural tensile strength of 73.3 and 6.5 MPa, respectively.

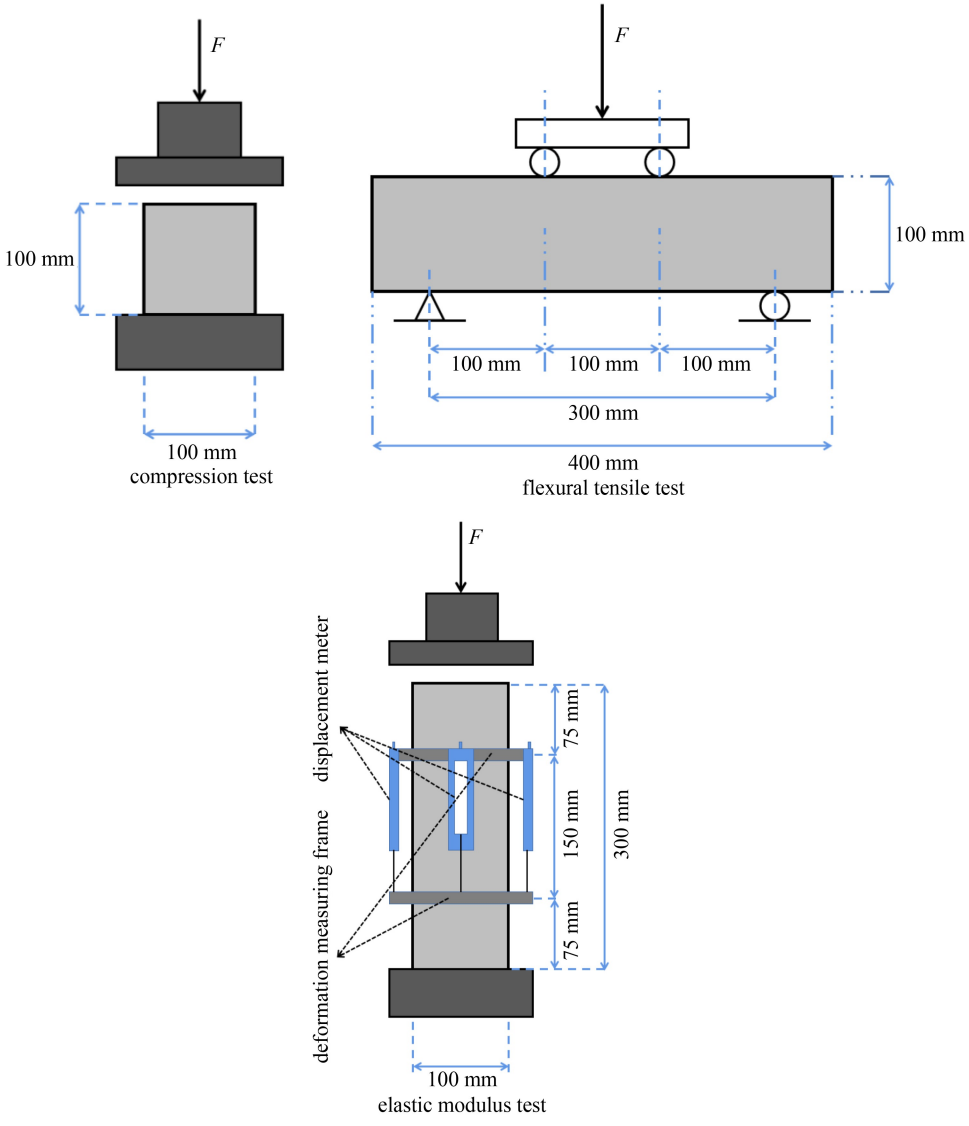

Fig. 8 The diagrammatic sketches of compression, flexural tensile, and elastic modulus test.

(a) (b) (c)

Fig. 9 Testing arrangement for TGC specimen: (a) compression, (b) flexural tensile, and (c) elastic modulus test.

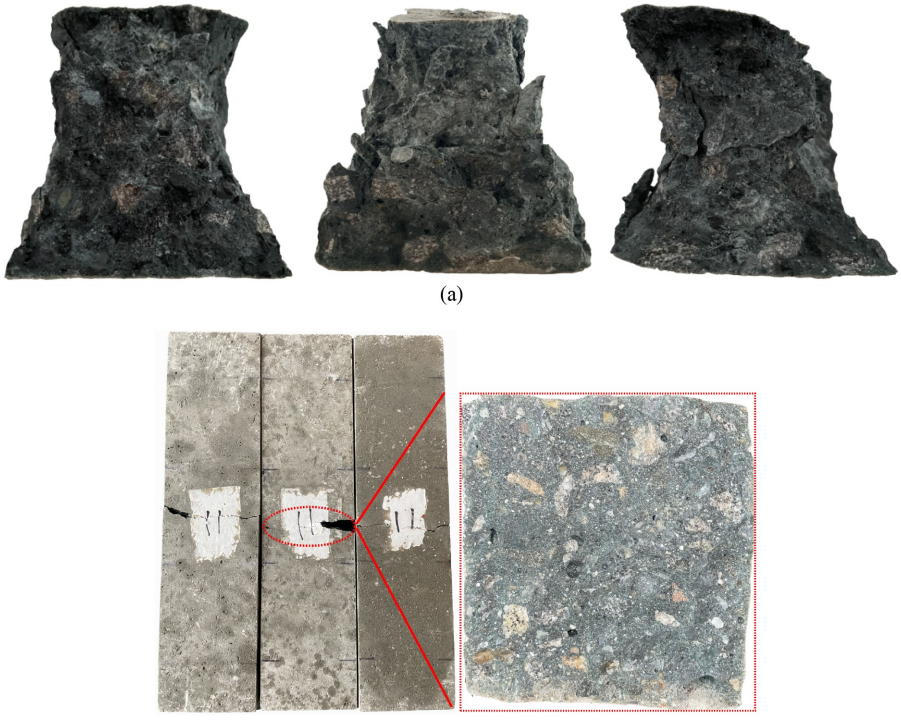

(a)

(b) (c)

Fig. 10 The failure pattern of TGC specimen. (a) Compression test; (b) flexural tensile test: breaking crack; (c) breaking section.

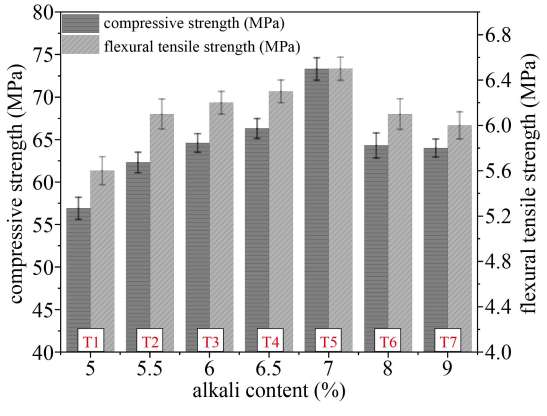

Fig. 11 The 28 d compressive strength and flexural tensile strength of TGC affected by AC.

The compressive strength of T5 was approximately 28.8% higher than that of T1, and the flexural tensile strength of T5 was approximately 16.1% higher than that of T1.

Figure 12 shows the 28 d compressive strength and flexural tensile strength of TGC prepared under the condition of constant AC with variable AAM. It also can be seen that there was variation of compressive strength and flexural tensile strength of TGC with different AAM values. The results shown in Fig. 12 indicate that the compressive strength of T13 was the lowest. Meanwhile, T8 and T13 had approximately equal values of flexural tensile strength. T8 obtained the minimum compressive strength of 60.1 and T8 and T13 both obtained the minimum flexural tensile strength of 5.9 MPa. When AAM reduced to 1.1, the compressive strength and

flexural tensile strength of T10 were both the highest compared to those of other specimens. T10 exhibited the maximum compressive strength and flexural tensile strength of 78.4 and 6.9 MPa, respectively. It can be seen that with decrease in AAM there was very little increment in the compressive strength and a remarkable increment in the flexural tensile strength. The compressive strength of T10 was approximately 30.4% higher than that of T13 and the flexural tensile strength of T10 was approximately 16.9% higher than that of T13.

3.2 Elastic modulus

Elastic modulus is a physical quantity that describes the elasticity of a material and a measure of its resistance to elastic deformation. As a vital performance parameter of engineering materials, the elastic modulus of TGC is worth studying. Therefore, the elastic modulus of TGC prepared with different AAM and AC was investigated in this paper. The variation trends of elastic modulus are shown in Fig. 13, which suggests that the elastic modulus varied with the variation of AAM and AC. When AAM was fixed at 1.4, the specimen of T1 attained the minimum value of elastic modulus, while the specimen of T5 attained the maximum value of elastic modulus. The elastic modulus of the specimen with AC of 7% was approximately 10.9% higher than that of the specimen with AC of 5%. This result indicates that the increase of AC with the appropriate range of 5% to 7% tended to improve the modulus of elasticity of TGC. When AC was fixed at 8%, the minimum value of elastic modulus was observed from T13. The elastic modulus of T8 was approximately equal to that of T13. T10 exhibited the maximum value of elastic modulus. The elastic modulus of the specimen with AAM of 1.1 was approximately 12.7% higher than that of the specimen with AAM of 1.5. This result indicates that the reduction of AAM with the appropriate range of 1.1 to 1.5 tended to improve the modulus of elasticity of TGC.

3.3 Experimental results

3.3.1 Mechanical properties

In the light of experimental results discussed above, within a certain range the increase of AC tends to improve the mechanical properties of TGC, but this enhancement is restrained when AC increases above that range. A similar phenomenon can also be observed with variation of AAM. An explanation for these observations is that the activity of geopolymer materials is rather low at room temperature, and sodium oxide can provide an appropriate alkaline environment to stimulate this activity. The strong alkalinity of sodium oxide can break the partial bonds of Ca-O, Si-O, and Al-O in the raw materials, and then the dissolved metal cations further

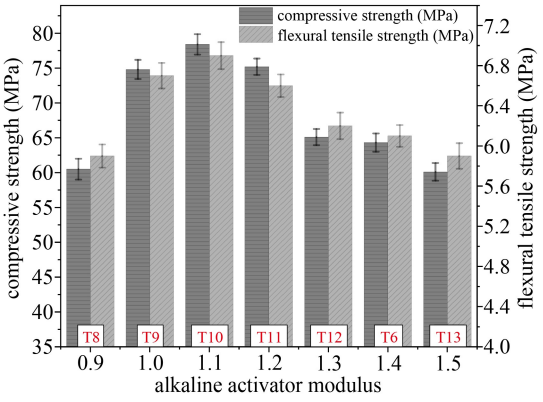

Fig. 12 The 28 d compressive strength and flexural tensile strength of TGC affected by AAM.

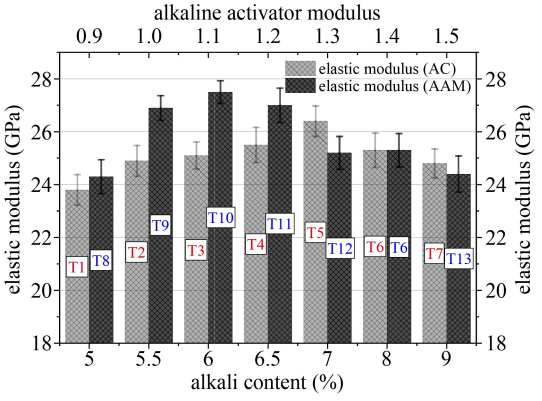

Fig. 13 The 28 d elastic modulus of TGC affected by AC and AAM respectively.

react with the silica in the sodium silicate solution to form C-S-H and C-A-S-H. So, when AC is deficient, the content of silica in solution is also small owing to invariant AAM. This means that the stimulation of the activator is weak and the amount of hydration reaction products is small on account of the small amount of silica in solution acting as a reactant. Therefore, the deficiency in the amount of sodium oxide is detrimental to the development of TGC strength. As the sodium oxide content increases, more Ca-O, Si-O, and Al-O bonds in the raw material are broken, more metal cations are dissolved into solution and hence the increase of hydration products which contribute to the overall strength growth of concrete [13,38]. This is the reason for rapid enhancement of strength. However, the content of sodium oxide has a specific range in which the rapid development of strength is facilitated. Silica will accordingly increase with the increase of sodium oxide due to constant AAM. In the case of increasing content of both sodium oxide and silica, inevitably, the stimulation and hydration reaction are rapidly accelerated, which makes the generation rate and amount of hydration products (C-(A)-S-H) on the surface of raw material particles faster and larger [38]. Increasing sodium oxide

content hinders the hydration reaction inside the hollow particles owing to more and more precipitation of geopolymer gels around the surface of particles, which eventually limits rapid strength development of the concrete. This is the reason for slowing development of strength with continuous increase of AC. And excessive AC has an unfavorable effect on strength of TGC. In addition, when AAM is at a low level, the silica content in the alkaline activator solution will increase with the increase of AAM. This tends to generate a more compact silicon-rich gel phase and enhance the strength of TGC [13,38]. However, with the continuous increase of AAM, the increase trend of strength becomes slower. These phenomena have also appeared in the researches of Cho et al. [38] and Qin et al. [13]. The above explanations are consistent with theirs.

In this study, when AAM is fixed at 1.4, the optimal threshold value of AC that plays a positive role in improving the mechanical properties of TGC is 7%. When AC is fixed at 8%, the optimal threshold value of AAM is 7%. Deterioration in strength occurs when the AC or AAM value is greater than the optimal threshold value.

3.3.2 SEM micrograph

In this paper, the fragments of crushed concrete specimen (T5, T8, and T10) were selected as the objects of SEM analysis and SEM micrographs are displayed in Fig. 14. As can be seen from Figs. 14(a)–14(c), the structures of T5 and T10 are more compact thanks to the sufficient quantity of geopolymer gels. However, the structure of T8, by contrast, is looser and geopolymer gels are scantier, probably due to the insufficient amount of silica in alkaline activator solution caused by low AAM. Loose structure caused by lower concentration of geopolymer gels has an adverse impact on the overall mechanical properties of concrete, and the mechanical property test results discussed in the above sections also reveal the possibility of the occurrence of this phenomenon. Figures 14(d)–14(f) show that fewer and finer cracks can be found in the micrographs of T5 and T10 at low magnification by comparison with T8. Therefore, considering the influence of AAM and AC discussed in the above sections on TGC, the mechanical properties of TGC can be improved under the condition of high AC and low AAM which are both in the specific range.

4 Assessment and prediction of mechanical properties of ternary geopolymer concrete

The variation of the flexural tensile strength and elastic modulus of TGC affected by AC and AAM were investigated above. To better assess the flexural tensile strength and elastic modulus of TGC, this paper cited several prediction models proposed in previous investigations to compare with the experimental values obtained in this study. The consequences and analyses of the comparison are discussed as below.

4.1 Assessment of flexural tensile strength using compressive strength

Experimental results discussed above manifested that

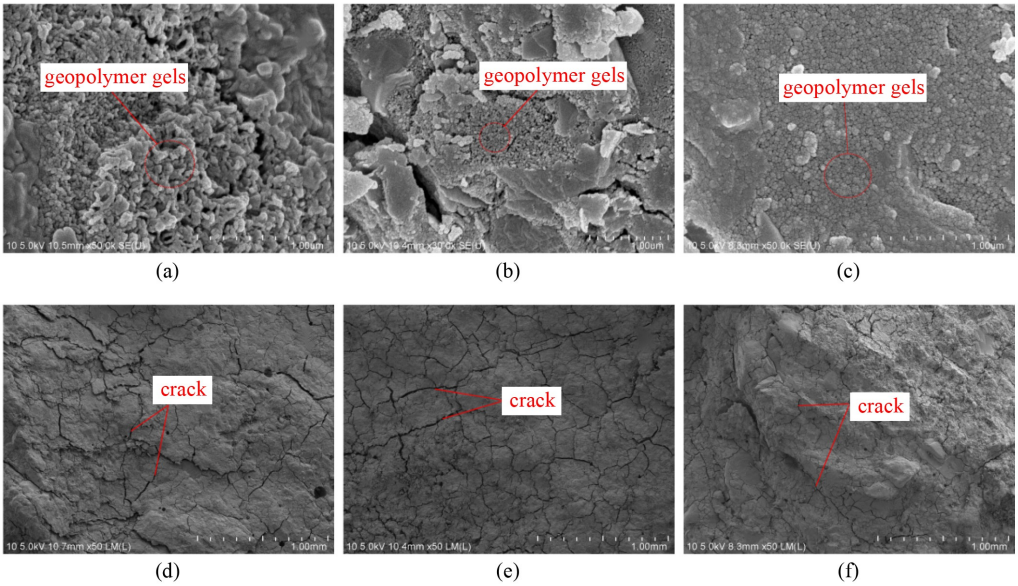

Fig. 14 The SEM micrographs of partial TGC fragments: (a) T5 with magnification of 50000, (b) T8 with magnification of 50000, (c) T10 with magnification of 50000, (d) T5 with magnification of 50000, (e) T8 with magnification of 50000 and (f) T10 with magnification of 50000.

there is a link between flexural tensile strength and compressive strength. The equations proposed by Australian standard (AS 3600-2009) [51] and other literatures were cited to predict the flexural tensile strength and compare with the experimentally determined values of the flexural tensile strength of TGC.

According to AS 3600-2009 [51], the approximate relationship between flexural tensile strength and compressive strength of OPC at 28 d is given by Eq. (2).

$$f_{cf} = 0.6 f_c^{0.5}, \tag{2}$$

where f_{cf} and f_c are flexural tensile strength and compressive strength of OPC at 28 d, respectively.

According to Nath and Sarker [52], flexural tensile strength of FA based geopolymer concrete can be calculated using Eq. (3).

$$f_{cf} = 0.93 f_c^{0.5}. \tag{3}$$

According to Waqas et al. [53], the flexural tensile strength of slag/FA geopolymer concrete can be calculated using Eq. (4).

$$f_{cf} = 0.25 f_c^{2/3}. \tag{4}$$

Figure 15 illustrates the ratios of predicted flexural tensile strength to test flexural tensile strength. The average values of respective ratios were indicated by dashed lines in the figure. Figure 15 shows that, in general, the ratios obtained by Eqs. (2) and (3) are both closest to 1 based on the differences, and the maximum of difference (0.34) between the mean of ratios and 1 can be observed from Eq. (4). It means that, under the same compressive strength, the difference between the value of flexural tensile strength predicted by Eq. (4) and actual value is largest compared with that predicted by other equations. The predicted and experimentally determined values of flexural tensile strength are also plotted in Fig. 16. As can be seen from Fig. 16, the experimentally measured values all fall in the middle of Eqs. (2) and (3) while Eq. (2) underrates the actual values and Eq. (3) overrates the actual values. Thus, an equation (Eq. (5), $R^2 = 0.945$) was investigated for the experimental flexural tensile strength of TGC, as shown in Fig. 16.

$$f_{cf} = 0.7646 f_c^{0.5}, \tag{5}$$

where f_{cf} is the flexural tensile strength of TGC at 28 d, and f_c is the compressive strength of TGC at 28 d.

4.2 Assessment of elastic modulus using compressive strength

CEB-FIP model code [54] and the equations recommended by previous researchers were utilized to predict the elastic modulus of TGC and compare with the experimentally determined elastic modulus of TGC at 28 d.

According to CEB-FIP model code [54], the 28 d elastic modulus of OPC can be calculated by the following equation:

$$E_c = 18275 (0.1 f_c)^{1/3}, \tag{6}$$

where E_c is the elastic modulus of OPC at 28 d. The

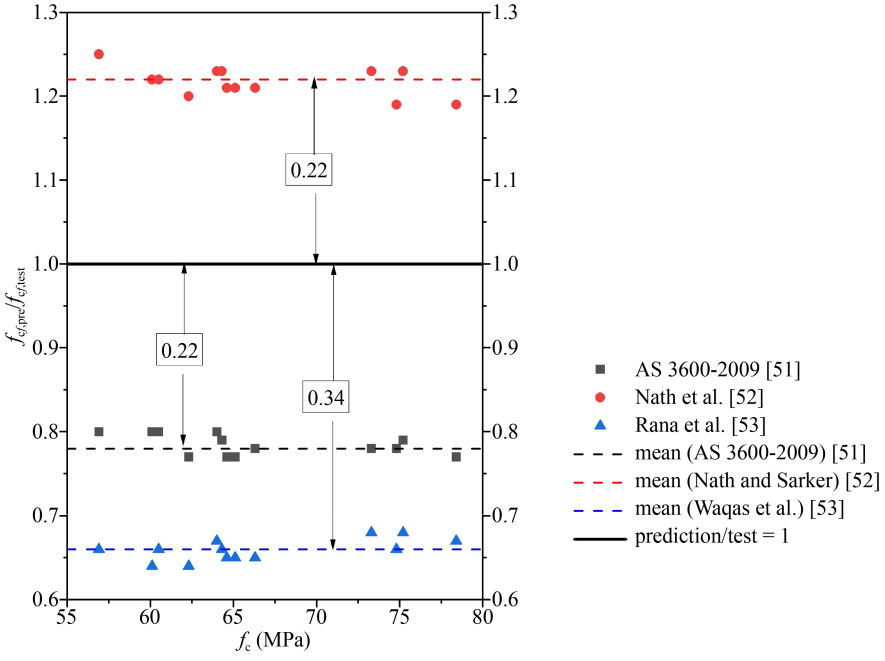

Fig. 15 The ratios of predicted flexural tensile strength to test flexural tensile strength obtained from AS 3600-2009 [51], Nath and Sarker [52], and Waqas et al. [53].

equation proposed by Nath and Sarker [52] is appropriate to predict the elastic modulus of FA based geopolymer concrete. The equation is shown below.

$$E_c = 3510 f_c^{0.5}. \quad (7)$$

A prediction equation suitable for slag/FA geopolymer concrete is proposed by Lee and Lee [55], as shown below.

$$E_c = 5300 f_c^{1/3}. \quad (8)$$

The ratios of predicted elastic modulus to test elastic modulus are plotted in Fig. 17. Figure 17 shows that the ratios obtained by Eq. (7) are the closest to 1, and the maximum of difference (0.35) between ratios and 1 can be observed from Eq. (6). The results indicate that, under the same compressive strength, the value of elastic modulus predicted by Eq. (7) provides the best fit to the actual value among these cited equations. The difference between ideal average value calculated by CEB-FIP model and actual average value of elastic modulus is the largest. The predicted and actual values of elastic modulus are also plotted in Fig. 18. As can be seen from the figure, the experimentally measured values all fall between Eqs. (7) and (8), much lower than Eq. (6) and closer to Eq. (7). However, Eq. (7) still overvalues the actual value, while Eq. (8) undervalues the actual value. The discrepancies observed above may be caused by different kinds of raw material composition, diverse parameters of activator or mix designs of concrete.

Considering that the two equations (Eqs. (7) and (8)) describing the development trend of elastic modulus above were obtained from normal strength concrete and the strength of concrete studied in this paper is higher than that of normal concrete, the models used to describe the development of elastic modulus of high strength concrete are cited, as shown below.

$$\text{American model [56]}: E_c = 3.32 f_c^{0.5} + 69. \quad (9)$$

$$\text{European model [57]}: E_c = 10 (f_c + 8)^{0.33}. \quad (10)$$

$$\text{Norwegian model [58]}: E_c = 9.5 f_c^{0.3}. \quad (11)$$

Also, the average values of the ratios and the differences are plotted in Fig. 19. Figure 19 shows that the differences between the mean values of the ratios calculated by each model and 1 are all extremely large. The maximum difference can reach 0.63. Figure 20 shows each high strength model and experimental values. It can be found that the elastic modulus of TGC is much lower than the values predicted by these high strength

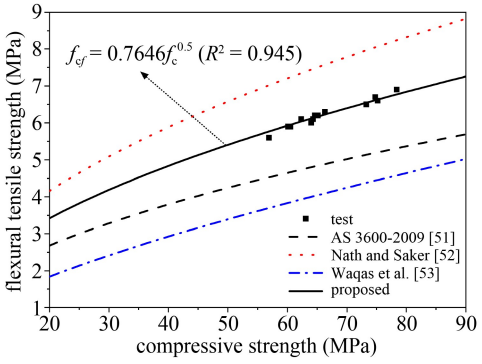

Fig. 16 Comparisons between predicted models (AS 3600-2009 [51], Nath and Sarker [52], and Waqas et al. [53]) and proposed model.

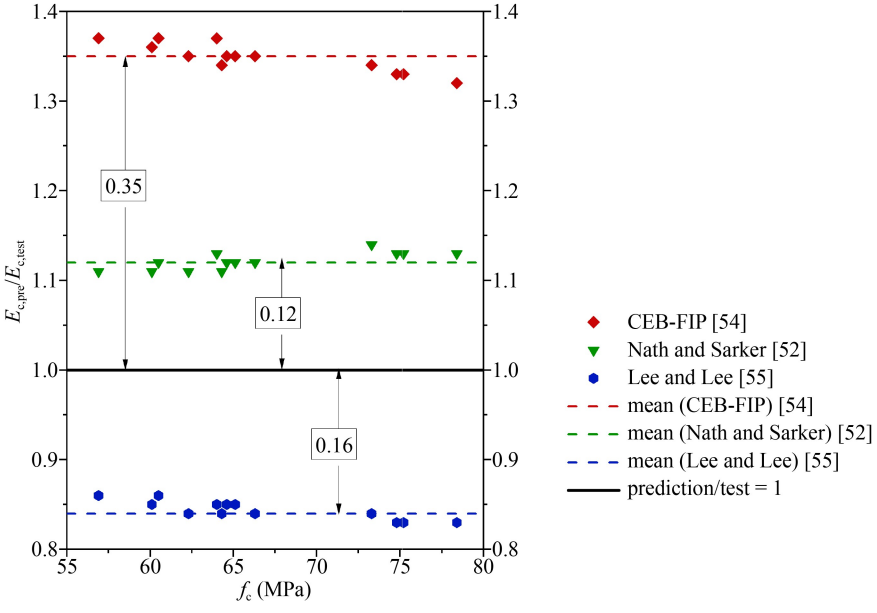

Fig. 17 The ratios of predicted elastic modulus to test elastic modulus obtained from CEB-FIP model [54], Nath and Sarker [52], and Lee and Lee [55].

concrete models. This indicates that all these models overrate the actual elastic modulus. Therefore, a properly fitting model is needed to predict the elastic modulus of TGC. In the light of the study of the elastic modulus of high strength concrete investigated by Ahmadi-Nedushan [59], the relationship between elastic modulus and compressive strength of concrete can be described in the following form.

$$E_c = a(f_c + b)^c + d,$$

where a, b, c, and d are constants.

Thus, an equation (Eq. (12), $R^2 = 0.987$), which can be used to predict elastic modulus from compressive strength, applicable to TGC is recommended in this paper, as shown in Figs. 18 and 20.

$$E_c = 2.261\,(f_c + 2.309)^{0.5373} + 3.511, \quad (12)$$

where E_c is the elastic modulus of TGC at 28 d, and f_c is the compressive strength of TGC at 28 d.

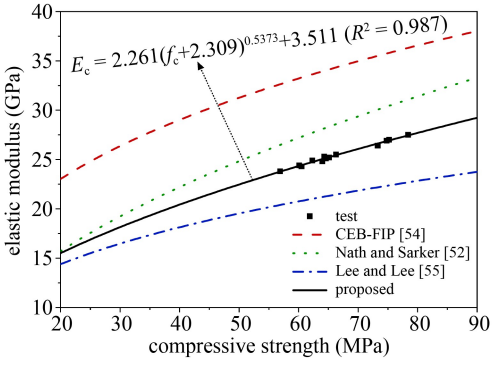

Fig. 18 Comparisons between predicted models (CEB-FIP model [54], Nath and Sarker [52], and Lee and Lee [55]) and proposed model.

4.3 Prediction of mechanical properties of ternary geopolymer concrete

In this study, the mechanical properties of TGC were investigated under the influence of different AAM and AC. In the above sections, the effects of varying AAM and AC of the alkaline activator on the mechanical properties of TGC and the assessment of the flexural tensile strength and elastic modulus of TGC have been discussed. In this section, the fitting models of compressive strength, flexural tensile strength and elastic modulus with respect to AAM and AC are investigated respectively. The fitting variation trend of mechanical properties are plotted in Figs. 21–23.

The functional equations (Eqs. (13)–(21)) for mechanical properties of TGC were fitted, shown below. The R-square coefficient (R^2) and covariance were used to check the fitting degrees of these equations.

The compressive strength (f_c), flexural tensile strength (f'_{cf}) and elastic modulus (E_c) of TGC with 1.4 AAM can be reasonably indicated by Eqs. (13)–(15), respectively in terms of AC, and each parameter value is given in Tables 3 and 4.

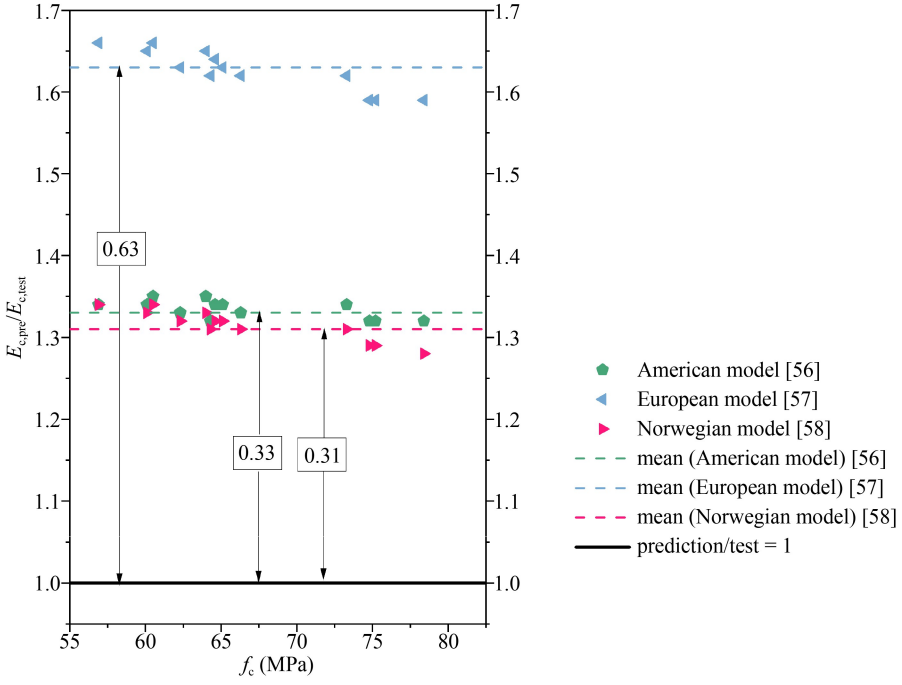

Fig. 19 The ratios of predicted elastic modulus to test elastic modulus obtained from American model [56], European model [57], and Norwegian model [58].

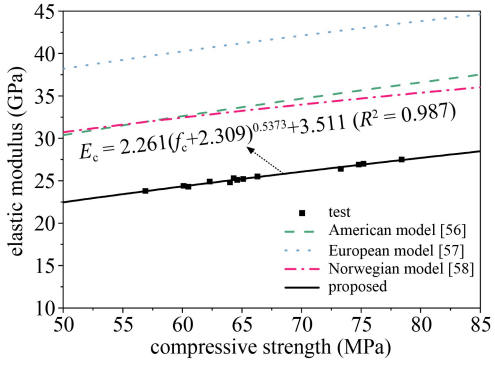

Fig. 20 Comparisons between predicted models (American model [56], European model [57], and Norwegian model [58]) and proposed model.

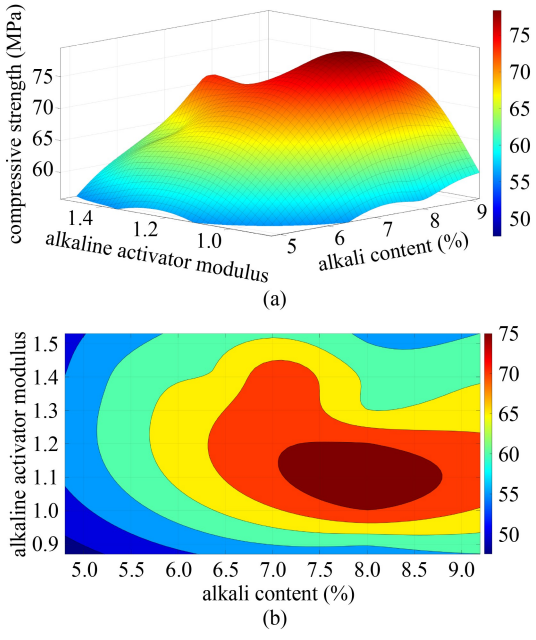

Fig. 21 The fitting variation trend of compressive strength under the combined effects of AC and AAM. (a) Three-dimensional image; (b) vertical view.

$$f_c = A_1*AC^4 + A_2*AC^3 + A_3*AC^2 + A_4*AC + A_5, \quad (13)$$

$$f_{cf} = B_1*AC^4 + B_2*AC^3 + B_3*AC^2 + B_4*AC + B_5, \quad (14)$$

$$E_c = C_1*AC^4 + C_2*AC^3 + C_3*AC^2 + C_4*AC + C_5. \quad (15)$$

Also, the compressive strength, flexural tensile strength and elastic modulus of TGC with 8% AC can be appropriately expressed by the following functional equations (Eqs. (16)–(18)) using AAM and each value of parameters is given in Table 5.

$$f_c = D_1*AAM^4 + D_2*AAM^3 + D_3*AAM^2 + D_4*AAM + D_5, \quad (16)$$

$$f_{cf} = E_1*AAM^4 + E_2*AAM^3 + E_3*AAM^2 + E_4*AAM + E_5, \quad (17)$$

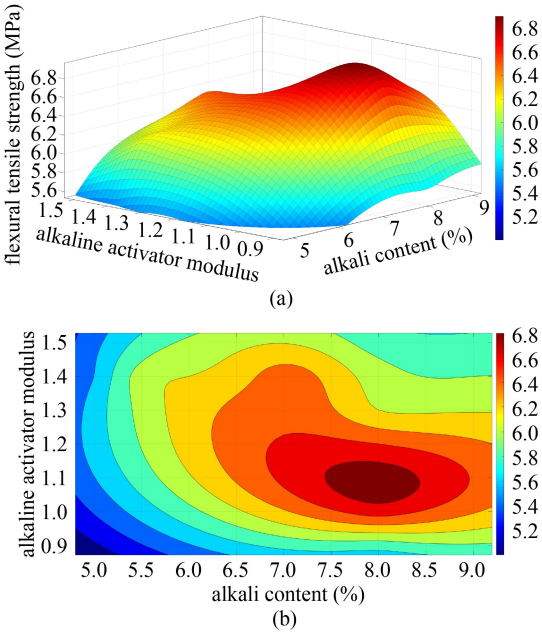

Fig. 22 The fitting variation trend of flexural tensile strength under the combined effects of AC and AAM. (a) Three-dimensional image; (b) vertical view.

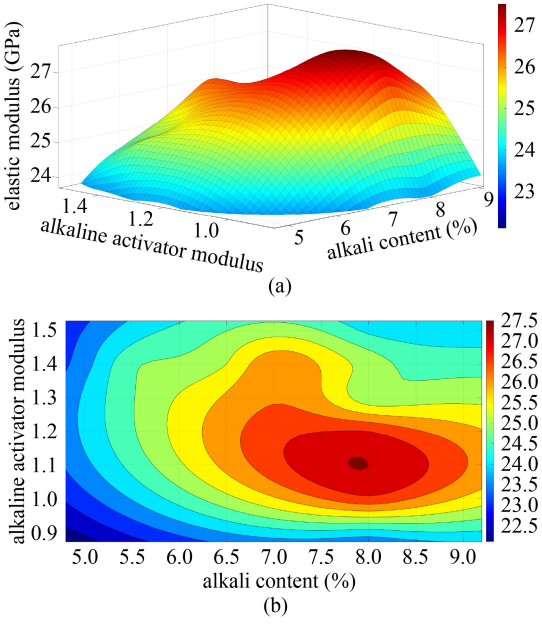

Fig. 23 The fitting variation trend of elastic modulus under the combined effects of AC and AAM. (a) Three-dimensional image; (b) vertical view.

$$E_c = F_1*AAM^4 + F_2*AAM^3 + F_3*AAM^2 + F_4*AAM + F_5. \quad (18)$$

Compressive strength, flexural tensile strength and elastic modulus, under the combined effect of AC and AAM on TGC, can be precisely predicted by quintic polynomials, as shown below. Meanwhile, parameters of quintic polynomials are shown in Table 5.

Table 3 Values of parameters, R^2 and covariance of Eqs. (13)–(15)

parameter	value	parameter	value	parameter	value
A_1	0.89	B_1	0.01	C_1	0.08
A_2	–24.48	B_2	–0.36	C_2	–2.06
A_3	245.20	B_3	3.00	C_3	20.34
A_4	–1062.00	B_4	–9.70	C_4	–85.58
A_5	1738.00	B_5	14.57	C_5	153.58
R^2	0.848	R^2	0.924	R^2	0.885
covariance	17.384	covariance	0.062	covariance	0.469

Table 4 Values of parameters, R^2 and covariance of Eqs. (16)–(18)

parameter	value	parameter	value	parameter	value
D_1	–651.52	E_1	–56.82	F_1	–174.24
D_2	3777.27	E_2	308.84	F_2	947.47
D_3	–8059.47	E_3	–623.45	F_3	–1915.68
D_4	7470.00	E_4	551.61	F_4	1699.27
D_5	–2460.73	E_5	–173.46	F_5	–529.78
R^2	0.965	R^2	0.985	R^2	0.951
covariance	47.736	covariance	0.137	covariance	1.407

Table 5 Values of parameters and R^2 of Eqs. (19)–(21)

parameter	value	parameter	value	parameter	value
z_0	–2843.26	z_1	–233.51	z_2	472.95
a_1	–96025.46	c_1	–3987.36	m_1	–18930.41
a_2	168845.55	c_2	7133.56	m_2	33339.93
a_3	–146136.92	c_3	–6263.35	m_3	–28923.09
a_4	62342.65	c_4	2704.26	m_4	12374.78
a_5	–10502.41	c_5	–460.23	m_5	–2091.73
b_1	18721.33	d_1	841.21	n_1	2884.59
B_2	–5694.71	d_2	–252.34	n_2	–871.71
b_3	857.48	d_3	37.53	n_3	130.43
b_4	–63.86	d_4	–2.77	n_4	–9.66
b_5	1.88	d_5	0.08	n_5	0.28
R^2	0.985	R^2	0.999	R^2	0.986
covariance	40.591	covariance	0.122	covariance	1.189

$$f_c = z_0 + a_1 * AAM + a_2 * AAM^2 + a_3 * AAM^3 + a_4 * AAM^4 + a_5 * AAM^5 + b_1 * AC + b_2 * AC^2 + b_3 * AC^3 + b_4 * AC^4 + b_5 * AC^5, \quad (19)$$

$$f_{cf} = z_1 + c_1 * AAM + c_2 * AAM^2 + c_3 * AAM^3 + c_4 * AAM^4 + c_5 * AAM^5 + d_1 * AC + d_2 * AC^2 + d_3 * AC^3 + d_4 * AC^4 + d_5 * AC^5, \quad (20)$$

$$E_c = z_2 + m_1 * AAM + m_2 * AAM^2 + m_3 * AAM^3 + m_4 * AAM^4 + m_5 * AAM^5 + n_1 * AC + n_2 * AC^2, + n_3 * AC^3 + n_4 * AC^4 + n_5 * AC^5. \quad (21)$$

Finally, the values predicted by above proposed equations (Eqs. (19)–(21)) were used to compare with experimental data collected from investigations of Waqas et al. [53] (slag/FA geopolymer concrete), Nath and Sarker [52] (FA geopolymer concrete) and Olivia and Nikraz [60] (FA geopolymer concrete). In the light of the mix proportions given by these papers, AAM (1.01–1.35) and AC (5.8%–8.1%) can be calculated. The comparisons are plotted in Figs. 24–26. It can be seen from these figures that the predicted compressive strength values are all significantly higher than the test compressive strengths of Waqas et al. [53], Nath and Sarker [52] and Olivia and Nikraz [60]. Only the flexural tensile strength of Olivia and Nikraz [60] is higher than the predicted flexural tensile strength. In contrast to the compressive strength and flexural tensile strength, the predicted elastic modulus is closer to the test elastic modulus of Waqas et al. [53] and Olivia and Nikraz [60], in general. However, the test elastic modulus of Nath and Sarker [52] is clearly lower than the predicted elastic modulus. Considering the actual condition, the difference between the test and predicted data can be attributed to the effects of other factors, such as the type and composition of geopolymer precursors, aggregate, curing methods and so on [61–63].

5 Conclusions

In this paper, the effects of AC and AAM on the mechanical properties of TGC were investigated and the SEM micrograph of the microstructure of TGC was analyzed. Then, appropriate prediction models for evaluating the mechanical properties of TGC were proposed. The main conclusions can be drawn as follows.

1) The increase of AC can provide alkaline environment for the geopolymerization of TGC and accelerate the dissolution rate of calcium oxide, alumina and silica in raw materials. Low AAM contains relatively low content of silica, which can prevent excessive precipitation of geopolymer gel on the surface of the raw material particle, so that the hydration process of particle can proceed evenly. In this study, when AAM was fixed at 1.4, the mechanical properties of TGC with 7% AC were the best. The mechanical properties of TGC with 1.1 AAM were the best when AC was fixed at 8%.

2) According to the SEM micrographs, TGC with higher AC and lower AAM had more compact structure constructed with geopolymer gels and fewer and finer internal cracks. This can be explained from the mechanisms of AC and AAM.

3) All the cited equations cannot precisely predict the

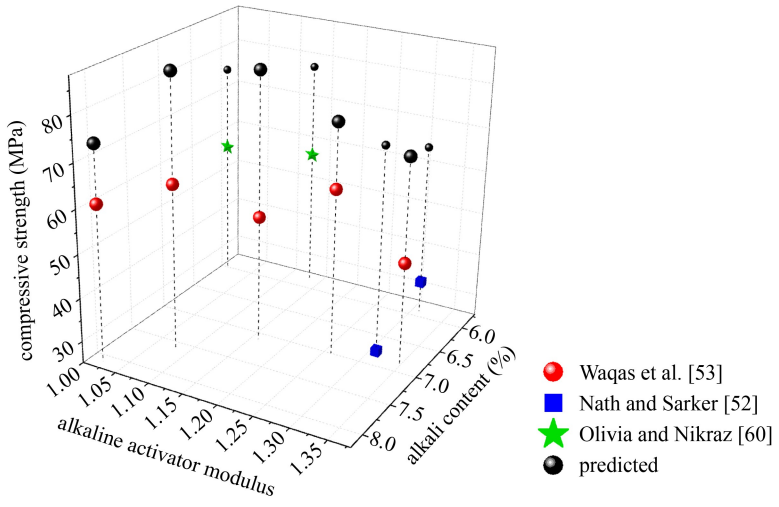

Fig. 24 Comparison of test compressive strength with predicted compressive strength.

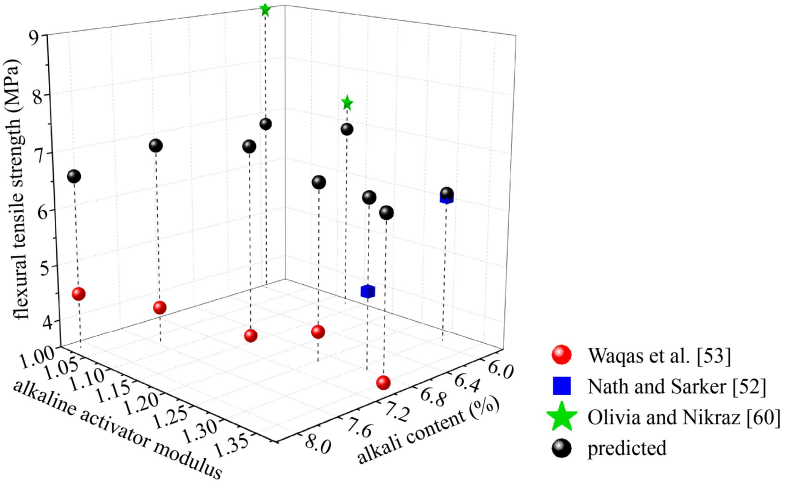

Fig. 25 Comparison of test flexural tensile strength with predicted flexural tensile strength.

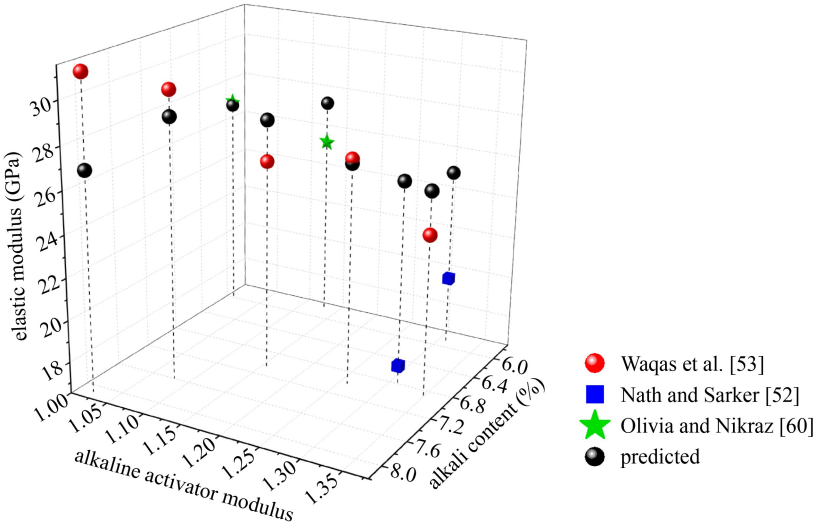

Fig. 26 Comparison of test elastic modulus with predicted elastic modulus.

flexural tensile strength and elastic modulus of TGC. Based on the test results of present investigation, Eqs. (5) and (12) were proposed to reasonably predict the flexural tensile strength and elastic modulus of TGC.

4) The combined effects of AC and AAM on the compressive strength, flexural tensile strength and elastic modulus of TGC were found to be predicted by Eqs. (19)–(21), respectively. By comparison with the experimental data of previous studies, it was found that other kinds of geopolymer concrete presented different mechanical properties from those of TGC. All these differences between the test and prediction can be attributed to various factors, such as the type and composition of geopolymer precursors, aggregate, curing methods and so on.

Acknowledgements This study was supported by the Fundamental Research Funds for the Central Universities (No. 2572021BJ01) and Heilongjiang Province Postdoctoral Foundation of China (No. LBH-Z20036).

References

1. Andrew R M. Global CO_2 emissions from cement production. Earth System Science Data, 2018, 10(1): 195−217
2. Cong P, Mei L. Using silica fume for improvement of fly ash/slag based geopolymer activated with calcium carbide residue and gypsum. Construction & Building Materials, 2021, 275(9): 122171
3. Liu Y W, Shi C J, Zhang Z H, Li N. An overview on the reuse of waste glasses in alkali-activated materials. Resources, Conservation and Recycling, 2019, 144: 297−309
4. Rashad A M, Khafaga S A, Gharieb M. Valorization of fly ash as an additive for electric arc furnace slag geopolymer cement. Construction & Building Materials, 2021, 294(2): 123570
5. Davidovits J. Geopolymers: Ceramic-like inorganic polymers. Journal of Ceramic Science and Technology, 2017, 8: 335−350
6. Rahman S S, Khattak M J. Roller compacted geopolymer concrete using recycled concrete aggregate. Construction & Building Materials, 2021, 283: 122624
7. Montemor M F, Cunha M P, Ferreira M G, Simões A M. Corrosion behaviour of rebars in fly ash mortar exposed to carbon dioxide and chlorides. Cement and Concrete Composites, 2002, 24(1): 45−53
8. Petlitckaia S, Gharzouni A, Hyvernaud E, Texier-Mandoki N, Bourbon X, Rossignol S. Influence of the nature and amount of carbonate additions on the thermal behavior of geopolymers: A model for prediction of shrinkage. Construction & Building Materials, 2021, 296: 123752
9. Ren J, Zhang L, San R. Degradation of alkali-activated slag and fly ash mortars under different aggressive acid conditions. Journal of Materials in Civil Engineering, 2021, 33(7): 04021140
10. Ren J, Sun H, Li Q, Li Z, Ling L, Zhang X, Wang Y, Xing F. Experimental comparisons between one-part and normal (two-part) alkali-activated slag binders. Construction & Building Materials, 2021, 309: 125177
11. Zhang S, Qi X, Guo S, Ren J, Chen J, Chi B, Wang X. Effect of a novel hybrid TiO_2-graphene composite on enhancing mechanical and durability characteristics of alkali-activated slag mortar. Construction & Building Materials, 2021, 275: 122154
12. Jindal B B, Alomayri T, Hasan A, Kaze C R. Geopolymer concrete with metakaolin for sustainability: A comprehensive review on raw material's properties, synthesis, performance, and potential application. Environmental Science and Pollution Research International, 2022, 1−26
13. Qin Y, Chen X, Li B, Guo Y, Niu Z, Xia T, Meng W, Zhou M. Study on the mechanical properties and microstructure of chitosan reinforced metakaolin-based geopolymer. Construction & Building Materials, 2021, 271: 121522
14. Yousef R I, El-Eswed B, Alshaaer M, Khalili F, Khoury H. The influence of using Jordanian natural zeolite on the adsorption, physical, and mechanical properties of geopolymers products. Journal of Hazardous Materials, 2009, 165(1−3): 379−387
15. Nath S K, Kumar S. Influence of iron making slags on strength and microstructure of fly ash geopolymer. Construction & Building Materials, 2013, 38: 924−930
16. Dehghani A, Aslani F, Ghaebi Panah N. Effects of initial sio2/al2o3 molar ratio and slag on fly ash-based ambient cured geopolymer properties. Construction & Building Materials, 2021, 293(7): 123527
17. Li C, Sun H, Li L. Reply to the discussion by John Provis of the review paper "A review: The comparison between alkali-activated slag (Si+Ca) and metakaolin (Si+Al) cements". Cement and Concrete Research, 2010, 40(12): 1768
18. Phoo-Ngernkham T, Maegawa A, Mishima N, Hatanaka S, Chindaprasirt P. Effects of sodium hydroxide and sodium silicate solutions on compressive and shear bond strengths of FA–GBFS geopolymer. Construction and Building Materials, 2015, 91: 1−8
19. Wu Y, Lu B, Bai T, Wang H, Du F, Zhang Y, Cai L, Jiang C, Wang W. Geopolymer, green alkali activated cementitious material: synthesis, applications and challenges. Construction and Building Materials, 2019, 224: 930−949
20. Nath P, Sarker P K. Effect of GGBFS on setting, workability and early strength properties of fly ash geopolymer concrete cured in ambient condition. Construction & Building Materials, 2014, 66: 163−171
21. Collins F, Sanjayan J. Workability and mechanical properties of alkali activated slag concrete. Cement and Concrete Research, 1999, 29(3): 455−458
22. Ehsan M, Tang W, Cui H. Chloride diffusion and acid resistance of concrete containing zeolite and tuff as partial replacements of cement and sand. Materials (Basel), 2017, 10(4): 372
23. Özen S, Alam B. Compressive strength and microstructural characteristics of natural zeolite-based geopolymer. Periodica Polytechnica. Civil Engineering, 2017, 62(1): 64−71
24. Rafeet A, Vinai R, Soutsos M, Sha W. Effects of slag substitution on physical and mechanical properties of fly ash-based alkali activated binders (AABS). Cement and Concrete Research, 2019, 122: 118−135
25. Villa C, Pecina E T, Torres R, Gomez L. Geopolymer synthesis using alkaline activation of natural zeolite. Construction & Building Materials, 2010, 24(11): 2084−2090
26. Poon C S, Lam L, Kou S C, Lin Z S. A study on the hydration rate of natural zeolite blended cement pastes. Construction & Building Materials, 1999, 13(8): 427−432
27. Perraki T, Kontori E, Tsivilis S, Kakali G. The effect of zeolite on

the properties and hydration of blended cements. Cement and Concrete Composites, 2010, 32(2): 128−133
28. Celerier H, Jouin J, Mathivet V, Tessier-Doyen N, Rossignol S. Composition and properties of phosphoric acid-based geopolymers. Journal of Non-Crystalline Solids, 2018, 493: 94−98
29. Rodríguez E D, Bernal S A, Provis J L, Paya J, Monzo J M, Borrachero M V. Effect of nanosilica-based activators on the performance of an alkali-activated fly ash binder. Cement and Concrete Composites, 2013, 35(1): 1−11
30. Brew D, Mackenzie K. Geopolymer synthesis using silica fume and sodium aluminate. Journal of Materials Science, 2007, 42(11): 3990−3993
31. Vinai R, Soutsos M. Production of sodium silicate powder from waste glass cullet for alkali activation of alternative binders. Cement and Concrete Research, 2019, 116: 45−56
32. Ren J, Zhang L, Walkley B, Black J R, San Nicolas R. Degradation resistance of different cementitious materials to phosphoric acid attack at early stage. Cement and Concrete Research, 2022, 151: 106606
33. Davidovits, Joseph. Geopolymer Cement: A Review 2013. Technical Papers 21. 2013
34. Ghafoor M T, Khan Q S, Qazi A U, Sheikh M N, Hadi M. Influence of alkaline activators on the mechanical properties of fly ash based geopolymer concrete cured at ambient temperature. Construction & Building Materials, 2020, 273(4): 121752
35. Kaya M, Uysal M, Yilmaz K, Atiş C D. Behaviour of geopolymer mortars after exposure to elevated temperatures. Materials Science—Medziagotyra, 2018, 24(4): 428−436
36. Atabey İ İ, Karahan O, Bilim C, Atiş C D. The influence of activator type and quantity on the transport properties of class F fly ash geopolymer. Construction & Building Materials, 2020, 264: 120268
37. Chindaprasirt P, Chalee W. Effect of sodium hydroxide concentration on chloride penetration and steel corrosion of fly ash-based geopolymer concrete under marine site. Construction and Building Materials, 2014, 63: 303−310
38. Cho Y K, Yoo S W, Jung S H, Lee K M, Kwon S J. Effect of Na_2O content, SiO_2/Na_2O molar ratio, and curing conditions on the compressive strength of FA-based geopolymer. Construction and Building Materials, 2017, 145: 253–260
39. Fernández-Jiménez A, Palomo A. Composition and microstructure of alkali activated fly ash binder: Effect of the activator. Cement and Concrete Research, 2005, 35(10): 1984−1992
40. Criado M, Fernández-Jiménez A, Palomo A, Sobrados I, Sanz J. Effect of the SiO_2/Na_2O ratio on the alkali activation of fly ash. Part II: 29Si MAS-NMR Survey. Microporous and Mesoporous Materials, 2008, 109(1−3): 525−534
41. Shahmansouri A A, Nematzadeh M, Behnood A. Mechanical properties of ggbfs-based geopolymer concrete incorporating natural zeolite and silica fume with an optimum design using response surface method. Journal of Building Engineering, 2021, 36: 102138
42. Ismail I, Bernal S A, Provis J L, San Nicolas R, Brice D G, Kilcullen A R, Hamdan S, van Deventer J S J. Influence of fly ash on the water and chloride permeability of alkali-activated slag mortars and concretes. Construction & Building Materials, 2013, 48: 1187−1201
43. Deb P S, Nath P, Sarker P K. The effects of ground granulated blast-furnace slag blending with fly ash and activator content on the workability and strength properties of geopolymer concrete cured at ambient temperature. Materials and Design, 2014, 62: 32–39
44. El-Hassan H, Elkholy S. Enhancing the performance of Alkali-Activated Slag-Fly ash blended concrete through hybrid steel fiber reinforcement. Construction & Building Materials, 2021, 311: 125313
45. Valipour M, Yekkalar M, Shekarchi M, Panahi S. Environmental assessment of green concrete containing natural zeolite on the global warming index in marine environments. Journal of Cleaner Production, 2014, 65: 418−423
46. Canpolat F, Yılmaz K, Köse M M, Sümer M, Yurdusev M A. Use of zeolite, coal bottom ash and fly ash as replacement materials in cement production. Cement and Concrete Research, 2004, 34(5): 731−735
47. Aiken T A, Kwasny J, Sha W, Tong K T. Mechanical and durability properties of alkali-activated fly ash concrete with increasing slag content. Construction & Building Materials, 2021, 301: 124330
48. Prusty J K, Pradhan B. Multi-response optimization using taguchi-grey relational analysis for composition of fly ash-ground granulated blast furnace slag based geopolymer concrete. Construction & Building Materials, 2020, 241: 118049
49. Sabet F A, Libre N A, Shekarchi M. Mechanical and durability properties of self consolidating high performance concrete incorporating natural zeolite, silica fume and fly ash. Construction & Building Materials, 2013, 44: 175−184
50. GBT 50081-2019. Standard For Test Methods of Physical and Mechanical Properties of Concrete. Beijing: General Administration of Quality Supervision, Inspection and Quarantine of the People's Republic of China, 2019 (in Chinese)
51. AS 3600-2009. Concrete Structures. Sydney: Standards Australia, 2009
52. Nath P, Sarker P K. Flexural strength and elastic modulus of ambient-cured blended low-calcium fly ash geopolymer concrete. Construction & Building Materials, 2017, 130: 22−31
53. Waqas R M, Butt F, Zhu X, Jiang T, Tufail R F. A Comprehensive study on the factors affecting the workability and mechanical properties of ambient cured fly ash and slag based geopolymer concrete. Applied Sciences (Basel, Switzerland), 2021, 11(18): 8722
54. CEB-FIP. Model Code. Lausanne: Comite Euro-International Du Beton, 1990, 1990
55. Lee N K, Lee H K. Setting and mechanical properties of alkali-activated fly ash/slag concrete manufactured at room temperature. Construction & Building Materials, 2013, 47: 1201−1209
56. Russell H G, Anderson A R, Banning J O, Cantor I G, Carrasquillo R L, Cook J E, Frantz G C, Hester W T, Saucier K L, Aitcin P C, Anderson F D. State-of-the-Art Report on High Strength Concrete. ACI Committee 363. 1984
57. CEB-FIP. Bullettin d'information 213/214 CEB-FIP Model Code 1990. London: Thomas Telford: 1993
58. Norwegian Council for Building Standardization. Concrete

Structures Design Rules NS 3473. Oslo: Norwegian Concrete Association, 1992

59. Ahmadi-Nedushan B. Prediction of elastic modulus of normal and high strength concrete using ANFIS and optimal nonlinear regression models. Construction & Building Materials, 2012, 36: 665−673
60. Olivia M, Nikraz H. Properties of fly ash geopolymer concrete designed by Taguchi method. Materials & Design, 2012, 36: 191−198
61. Farooq F, Jin X, Faisal Javed M, Akbar A, Izhar Shah M, Aslam F, Alyousef R. Geopolymer concrete as sustainable material: A state of the art review. Construction & Building Materials, 2021, 306: 124762
62. Farhan K Z, Johari M A M, Demirboğa R. Assessment of important parameters involved in the synthesis of geopolymer composites: A review. Construction & Building Materials, 2020, 264: 120276
63. Jindal B B. Investigations on the properties of geopolymer mortar and concrete with mineral admixtures: A review. Construction & Building Materials, 2019, 227: 116644